



Ground penetrating radar (GPR) models of the regolith and water reservoir of an underground dam in the Brazilian semiarid region

Gustavo M. Vasques ^{a,*}, Hugo M. Rodrigues ^{a,b}, Emanuel Huber ^c, Sílvio R.L. Tavares ^a, Flávio A. Marques ^a, Maria Sônia L. Silva ^a

^a Embrapa Solos, Rua Jardim Botânico, 1024, Jardim Botânico, Rio de Janeiro 22460-000, Brazil

^b Universidade Federal Rural do Rio de Janeiro, Departamento de Solos, Rodovia BR 465 km 7, Seropédica 23890-000, Brazil

^c University of Basel, Department of Environmental Sciences, Bernoullistrasse 32, Basel 4056, Switzerland



ARTICLE INFO

Keywords:

Near-surface geophysics
Exploration geophysics
Impermeable layer
Spatial interpolation

ABSTRACT

Underground dams supply water for smallholders in semiarid regions. The aim was to use a ground penetrating radar (GPR) to detect and map the depth to the regolith, validate the size and position and calculate the water reservoir volume of a future underground dam. A GPR survey using a 450 MHz antenna was conducted across an intermittent stream bed in a 0.85-ha area in northeastern Brazil. Nine soil trenches were opened, and the depth to the regolith was recorded at each site. The radargrams were pre-processed, migrated, and the features corresponding to the top of the regolith were delineated in the radargrams. The regolith and the terrain surface were interpolated and plotted in 3D, and the underground water reservoir volume was estimated. The depth to the regolith ranged from 0.81 to 1.60 m at the soil sites, with larger values observed along the intermittent stream thalweg, and close to the dam at the lowest part of the terrain. The radargrams transverse to the slope suggest that the future dam should be 45 m longer and centered at the thalweg position, 22 m south of the initially proposed location. This would increase the water reservoir by 50% to a total of 6 million L. The GPR allowed to properly locate the future underground dam, visualize its shape in 3D and estimate its water reservoir volume, with minimal need of soil sounding.

1. Introduction

The largest continuous semiarid region in the world is located in the northeast of Brazil and spans about 1 million km². This area occupies 12.5% of the Brazilian territory, comprises 1262 municipalities, and hosts 27 million people, which correspond to 13% of the population of Brazil. This region has one of the lowest human development indexes in South America, mostly due to the scarcity and irregularity of rainfall, which hinders the development and well-living of the rural population. The low water availability is clear from the high annual water deficit, with an average rainfall of 300 to 750 mm year⁻¹ and reference evapotranspiration of 1504 to 2414 mm year⁻¹ (Cabral Júnior and Bezerra, 2018). The situation is aggravated by the absence of perennial rivers that could provide freshwater for human use.

In arid and semiarid regions, where surface water sources are scarce or non-existent, groundwater may be the only option to provide water for human consumption and other uses throughout the year (Onder and Yilmaz, 2005). However, existing water reservoirs are few and are based

on technology for capturing and storing water above the ground by small dams, where water is lost by evaporation. Typically, the water stored in these dams is used for human consumption, animal watering, and irrigation. As an alternative, underground dams have been developed and used to bar and store rainwater in the subsurface, minimizing evaporation (Ishida et al., 2003, 2011; Lima et al., 2018; Lopes et al., 2013; Silva et al., 2010). The water stored by the underground dam can be pumped or drained out and used for human consumption, other domestic activities, as water supply for farm animals (for example, chicken, cattle, horses, goats), and/or for irrigation (typically fruits and vegetables). The water can also be used for cropping directly in the water accumulation area upstream of the dam, in which case the water stored in the soil pores is accessed by the crop roots.

Underground dams have been used to store rainwater and supply water for family farming in Brazil's semiarid region (Silva et al., 1998, 2009; Ximenes et al., 2019). Due to their simplicity, the construction and maintenance of underground dams are relatively cheap, offering a low-cost alternative for the farmers' yearlong water supply, especially for

* Corresponding author.

E-mail address: gustavo.vasques@embrapa.br (G.M. Vasques).



Fig. 1. Underground dam construction process, showing: (A) The trench dug across the drainage line, with the outlying wall covered with plastic sheet; and (B) A tractor filling the trench with the earth that was previously removed. Source: Flávio A. Marques.

smallholders. Besides, there is no need to flood the land, making the areas upstream of the dams manageable for agriculture (Silva and Porto, 1982). This water capture technology is present in the semiarid region of Brazil and countries in Africa and Asia, such as Mali (Forzieri et al., 2008), Kenya (Ertsen and Hut, 2009; Quilis et al., 2009), Turkey (Apaydin, 2009) and Saudi Arabia (El-Hames, 2012).

Underground dams work by blocking the horizontal flow of the rainwater through the subsurface soil, and accumulating and storing the water in the soil pores. The dam can be built from the ground level or have a wall aboveground to also block and store surface water for a short period (up to about 2 to 3 months after the rainy season). The underground dam is installed in areas of convergent natural drainage. To intercept underground water flow, a trench is dug transversal to the water flow to the depth of the impermeable layer or rock. The outlying trench wall is covered by a 200 µm-thick impermeable polyethylene plastic sheet (Fig. 1A). Then, the trench is closed with the earth that was previously removed (Fig. 1B). To maximize water accumulation and avoid lateral leakage, the shape of the underground impermeable layer must be known, and the dam must be long enough to block the water flow across the drainage line.

Lima et al. (2013) discussed different methods for building underground dams and some criteria for adequately locating and sizing underground dams considering each family's purpose and demand. In general, according to the authors, underground dams should be built in areas where the depth to the regolith lies between 1 and 3.5 m, the soil

has a medium to sandy texture, and the average slope gradient in the catchment area is below 2%. However, despite its importance, the volume of water stored by the underground dam is typically not quantified. This is due to the high cost of measuring and mapping the impermeable layer beneath the soil that limits the vertical flow of water at the bottom of the reservoir. This layer may consist of saprolite, regolith or solid rock. Its assessment and mapping across the dam's accumulation area requires drilling and opening soil trenches, making the process costly, and thus, hardly ever done (Doolittle et al., 2006).

The ground penetrating radar (GPR) may be an efficient alternative for mapping soil restrictive layers in the subsurface (Bristow and Jol, 2003; Freeland et al., 1998; Gerber et al., 2010; Loperte et al., 2011; Pueyo Anchuela et al., 2018). The GPR is a geophysical sensor that measures variations in the dielectric constant (relative permittivity) of the soil caused by high-frequency electromagnetic waves (1 MHz to 1 GHz) that are emitted and received by the GPR antenna. It generates 2D images (radargrams) of the soil profile in depth along a travelled path. The resolution and maximum depth of the radargrams vary according to the antenna frequency, where higher frequencies increase the resolution and decrease the depth of penetration (Daniels, 1989). When georeferenced, radargrams obtained in different directions in the same area can be combined to generate 3D images for detecting and mapping buried targets, depositional features (Castro et al., 2014; Lima et al., 2018; Sass, 2007), and other features of interest. For this, methods for acquiring, processing, and interpreting radargrams are applied using specific software. An on-site survey of the underground features of interest must be done serving as ground truth for processing the radargrams and/or validating the results.

Lima et al. (2018) used GPR to allocate underground dams in the semiarid region of the Rio Grande do Norte state in northeastern Brazil. They made several cross-sectional radargrams along the alluvial body of an intermittent stream bed and used 3D modeling to delineate the stream bed and the bedrock underneath. The interpreted radargrams showed an ideal location to place the dam that maximized the area of water accumulation and minimized the construction cost. Ground penetrating radar has also been used to characterize soil mapping units (Doolittle, 1982), identify soil class boundaries (Nascimento et al., 2019a), identify the depths of horizons with abrupt textural transitions (Nascimento et al., 2019b; Rodrigues et al., 2019), and map soils in high resolution (Davis and Annan, 1989). Fan et al. (2020) reviewed the literature on geophysical methods applied to water infiltration in soils, covering the visualization of infiltration-related structures, including bedrock and soil restrictive layers. Based on Fan et al. (2020), the lack of GPR studies to identify and map soil restrictive layers is evident. Douglas et al. (1992), Knight (2001), and Liu et al. (2016) provide an overview of GPR for other environmental applications.

Afshar et al. (2017) used GPR to identify the petrosaline horizon (a layer cemented by soluble salts) in arid and semiarid areas in southeastern Iran. One of the most important factors affecting soil depth in arid regions is the consolidated pedogenic and cemented horizons, such as the petrocalcic, petrosaline, duripan, and petrogypsic horizons. They used a 250 MHz shielded antenna in common offset mode and sampled across ten parallel transects 100-m long and 10-m apart in two locations. The cemented horizons showed greater compaction, fewer pores, and a higher apparent density than the adjacent layers. The depth range of the identified petrosaline horizon was 0.12–0.40 m, and the predicted average depths were 0.35 m from GPR data, and 0.25 m from field samples. Nováková et al. (2013) used GPR on Czech Cambisols and Stagnosols to identify the soil horizons and their spatial position. They coupled the GPR survey with vertical electric sounding (VES) to detect rocks and assess their degree of weathering. The radargrams showed contrasting redoximorphic and R horizon boundaries, but did not show clear boundaries for the C horizons of Cambisols. In a study to identify suitable sites for underground dams in southeastern Brazil, Gomes and Vieira (2020) used VES to visualize and characterize the subsurface structures close to an intermittent stream. They identified low-resistivity

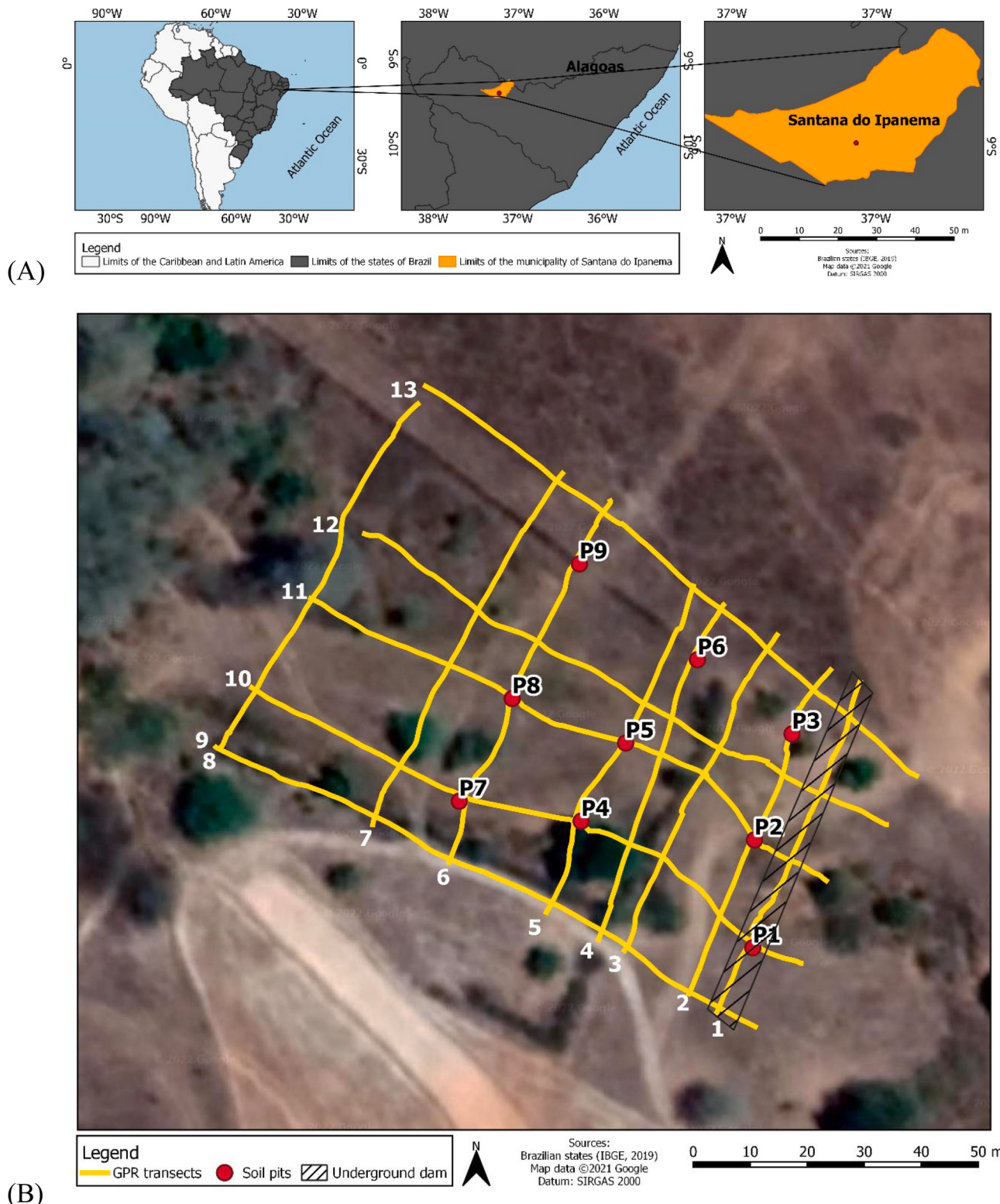


Fig. 2. (A) Location of the study area; (B) Location of the ground penetrating radar (GPR) survey transects (1 to 13), soil sites (P1 to P9), and proposed length and location of the future underground dam (hatched feature). Source of Brazilian state boundaries: Instituto Brasileiro de Geografia e Estatística ([IBGE, 2019](#)).

(< 800 Ωm) soil layers – a clayey one (< 150 Ωm) on the stream banks and a sandy one (< 800 Ωm) on the stream channel – lying above a high-resistivity (> 1000 Ωm) bedrock.

The lack of research using GPR and 3D processing tools to identify and map soil restrictive layers to assist in allocating underground dams and estimating their water reservoir volume is noteworthy. Geophysical

research using free and open-source software for processing, visualizing and interpreting GPR data is even less common. Thus, there is an opportunity to advance the use of GPR, without the need for expensive software and black-box routines, for underground dam allocation and assessment and other applications.

The objectives of this study were to use GPR and free and open-



Fig. 3. (A) Ground penetrating radar in the foreground and trench digging for soil description and classification in the background; (B) Soil profile P9 classified as *Neossolo Rególico Eutrófico léptico* (Regosols; Psammets). Source: Gustavo M. Vasques.

source software to: (a) map the surface terrain; (b) identify and map the depth to the regolith; (c) validate the proposed size and location of the dam; and (d) estimate the water reservoir volume of an underground dam to be built in Santana do Ipanema, Alagoas state, in the semiarid region of northeastern Brazil.

2. Materials and methods

2.1. Study area

The study was carried out in an experimental area of the Federal Institute of Alagoas in the municipality of Santana do Ipanema, Alagoas state, in the *Caatinga* (semiarid) biome in northeastern Brazil. The study area has about 0.85 ha and central latitude and longitude 9°23'46.5" S and 37°13'39.4" W, respectively (Fig. 2A). According to the Köppen classification, it has a BSh and BWh climate, with high annual temperatures, low rainfall ranging between 400 and 900 mm (Barros et al., 2012), in addition to low relative humidity.

The area is located at the low São Francisco river pediplain and is part of the *Canindé* geologic domain, mainly comprised of granites and gneisses (Araújo Filho et al., 2020). The lithology of the area consists of river deposits, and the soils include *Neossolos Fluvicos* (Fluvisols; Fluvents), *Neossolos Rególicos* (Regosols; Psammets), and *Planossolos Háplicos* (Planosols; Aqualfs). These soils typically occur in similar relief and geological settings in the region. The *Neossolos Fluvicos* derive from colluvial-alluvial sediments that accumulate close to drainage channels. The layers that make up the soil usually present great variations in morphological, physical and chemical attributes, including particle size distribution and porosity. The *Neossolos Rególicos* occur typically in the Brazilian semiarid region and usually present sandy texture, as well as primary minerals in the sand and coarser particle size fractions. The *Planossolos Háplicos* are imperfectly to poorly drained soils that present an argillic B horizon underlying an A or E horizon. Their B horizons are compact, very hard when dry and have considerably more clay than the upper horizons (Araújo Filho et al., 2020).

An area with <3% slope gradient was selected around an intermittent stream as the location for building the underground dam. Initially, it

is proposed that the underground dam be built in the intermittent stream's thalweg (central) position at the lower part of the slope at the eastern end of the study area. The proposed length of the dam corresponds to the GPR transect 1 (Fig. 2B, hatched feature). The proposed size and location of the dam will be validated by this study.

2.2. Description and classification of soils

Trenches up to 3-m deep were opened at nine sites close to the GPR transects (Fig. 3B, P1 to P9) to assess horizontal and vertical soil variation and identify the depth to the regolith across the study area. Soil profiles were described according to Santos et al. (2015) and classified according to the Brazilian Soil Classification System (Santos et al., 2018). The described and classified soil profiles were used to identify the subsurface features of interest, allowing interpreting and further processing of the radargrams.

2.3. GPR data acquisition and processing

The GPR used was the MALÅ GroundExplorer (Guideline Geo AB, Sundbyberg, Sweden), mounted on an all-terrain cart equipped with an odometer, GPS receiver, and a 450 MHz shielded monostatic antenna (Fig. 3A) that allowed readings to an approximately 4-m depth. The GPR data were acquired along 13 transects, with five transects parallel to the slope (top-to-dam direction) and eight transverse to the slope (Fig. 2B), to represent the variation of the subsurface in the study area.

The GPR data (radargrams) were processed using the RGPR package (Huber and Hans, 2019) in R (R Core Team, 2020). The 13 radargrams were processed by applying a sequence of filters to attenuate the noise and increase the contrast for viewing the features of interest, including (RGPR functions in parentheses): Zero-time estimate (*estimateTime0*); Zero-time correction (*time0Cor*); Low-frequency noise removal (*dewow*); Gain correction (*gain*); Automatic gain correction (*gain*); Eigenvalue filtering (*eigenFilter*); and Constant spacing correction (*timeCorOffset*). The average speed of propagation of the electromagnetic wave was then estimated at 0.17 cm ns^{-1} by matching the top of the regolith identified in the described soil profiles to their corresponding positions in the

Table 1

Taxonomic classes, surface elevation and depth to the regolith at the soil sites.

Soil site	Brazilian Soil Classification System ¹	FAO WRB ²	Soil Taxonomy ³	Terrain surface elevation (m)	Depth to the regolith (cm)
P1	<i>Neossolo Rególico eutrófico típico</i>	Regosols	Psammments	207	120
P2	<i>Neossolo Flúvico eutrófico típico</i>	Fluvisols	Fluvents	205	120
P3	<i>Neossolo Rególico eutrófico típico</i>	Regosols	Psammments	203	130
P4	<i>Planossolo Háplico eutrófico solódico</i>	Planosols	Aqualfs	207	110
P5	<i>Neossolo Flúvico eutrófico típico</i>	Fluvisols	Fluvents	205	160
P6	<i>Neossolo Rególico eutrófico típico</i>	Regosols	Psammments	204	100
P7	<i>Neossolo Flúvico eutrófico típico</i>	Fluvisols	Fluvents	208	150
P8	<i>Planossolo Háplico eutrófico solódico</i>	Planosols	Aqualfs	207	94
P9	<i>Neossolo Rególico eutrófico léptico</i>	Regosols	Psammments	207	81

¹ IUSS Working Group WRB (2015).² Santos et al. (2018).³ Soil Survey Staff (2014).

radargrams. The *setVel* function of the RGPR package was used for this.

The coordinates and elevation data obtained by the GPS embedded in the GPR were used to migrate the radargrams using the Kirchhoff method (Dujardin and Bano, 2013) implemented by the *migrate* function of the RGPR package. The migration process relocates the GPR data vertically to match the terrain topography and recovers the actual shape of the radargram features by correcting the distortions caused by reflections from buried objects, dips, and irregularities with contrasting permittivity.

After processing the radargrams, the regolith features became more evident and were outlined using the *delineate* function. The depth to the regolith delineated in the radargrams was confirmed by pairing the radargrams spatially with their corresponding positions in the soil profiles using the *closestTr* and *relTrPos* functions. The delineation process returns a table with the latitude, longitude and elevation of the delineated feature, in this case, the top of the regolith, which corresponds to the bottom of the water accumulation area.

The regolith features outlined in all radargrams were grouped and interpolated by the *interp2DDelineations* function to derive latitude, longitude and elevation values for the top of the regolith. Then, the

elevation of the top of the regolith, that is, the bottom of the water reservoir, was interpolated to a 2-m spatial resolution (pixel size) grid across the accumulation area using multilevel B-splines imported from the MBA package (Finley et al., 2017) and implemented by the *spinInterpToRaster* function of the RGPR package. The terrain surface elevation, represented by the upper limit of the radargrams after zero-time correction and migration, was also interpolated using the same procedure and settings.

2.4. Volume of the water reservoir

The water reservoir volume was calculated by multiplying the volume of the underground dam water accumulation area, that is, the soil volume in the accumulation area, by the soil porosity. It was assumed that a single porosity value can approximate the soil porosity in the area and that all soil pores can be filled with water. Spatially, the accumulation area is limited at the top by the terrain surface elevation (z_{surf}) and at the bottom by the elevation of the top of the regolith (z_{reg}), both of which mapped with 2-m resolution (pixel size). The total water reservoir volume in the accumulation area was calculated using Eq. (1).

$$V = \sum_{i=1}^n 0.01 \times (z_{surf_i} - z_{reg_i}) \times res^2 \times p \quad (1)$$

Where: V is the total volume of the water reservoir, in m^3 ; z_{surf_i} and z_{reg_i} are the elevations, in m, of the terrain surface and the top of the regolith, respectively, in the i -th pixel among the n pixels covering the accumulation area of the future underground dam; res is the pixel size, in m; and p is the soil porosity, in %.

The value of the soil porosity (p) used was 38%. This value was calculated using data from soils from the same region with similar characteristics to the soils observed in the study area. The soils selected for the porosity estimation were taken from an exploratory soil survey of the Alagoas state (Jacomine et al., 1975) and consisted of four *Neossolo Flúvico* (Fluvisols; Fluvents), eight *Neossolo Rególico* (Regosols; Psammments), and 17 *Planossolo Háplico* (Planosols; Aqualfs) samples. A single porosity value was calculated for the whole accumulation area as a depth-weighted average of the soil porosity from the horizons of the 29 selected soil profiles using Eq. (2).

$$p = \sum_{i=1}^{n(i)} \left[\sum_{j=1}^{n(j)} p_{ij} \times w_{ij} \right] \left/ \sum_{j=1}^{n(j)} w_{ij} \right. \left/ n(i) \right. \quad (2)$$

Where: p is the soil porosity, in %; and p_{ij} and w_{ij} are the soil porosity, in %, and the thickness, in m, respectively, of the j -th horizon among the $n(j)$ horizons of the i -th soil profile among the $n(i)$ selected soil profiles ($n(i) = 29$).

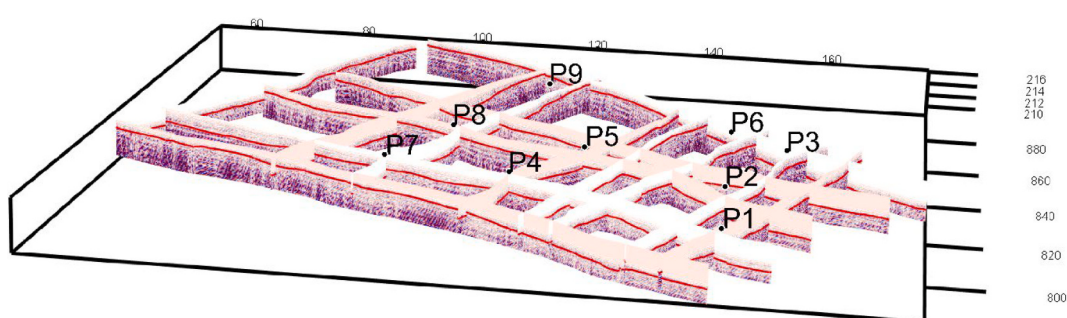


Fig. 4. Processed and migrated radargrams of the 13 survey transects showing the top of the regolith delineated as red lines. The coordinates are in meters. (For interpretation of the references to colour in this figure legend, the reader is referred to the web version of this article.)

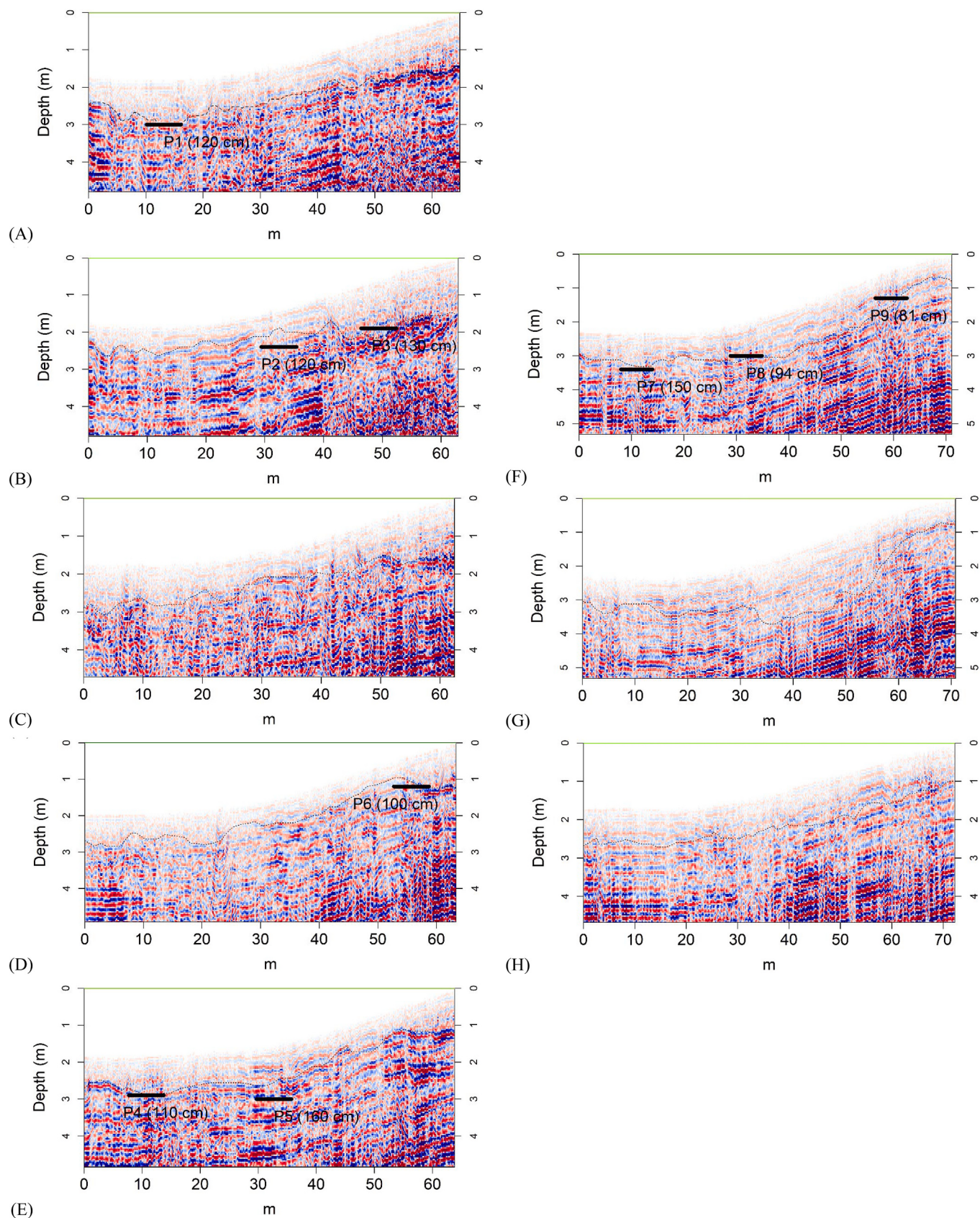


Fig. 5. Radargrams of the eight survey transects transverse to the slope showing the delineated top of the regolith as dashed black lines and its corresponding position observed at the soil sites as black dashes.

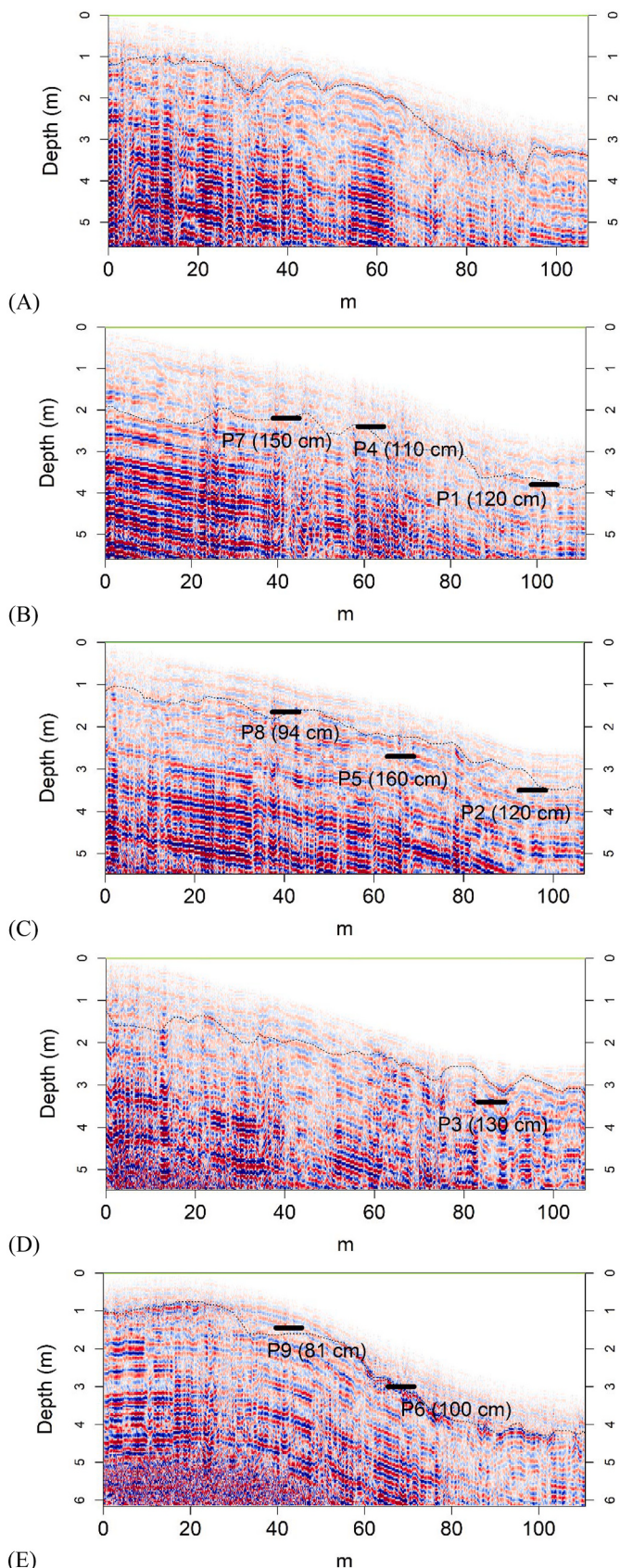


Fig. 6. Radargrams of the five survey transects parallel to the slope showing the delineated top of the regolith as dashed black lines and its corresponding position observed at the soil sites as black dashes.

3. Results and discussion

3.1. Soils and radargrams

Four soils were described as *Neossolo Rególico*, three as *Neossolo Flúvico* and two as *Planossolo Háplico* (Table 1). These soils are formed from colluvial-alluvial sediments and their variable texture and porosity along the profile result from weaker or stronger rains that bring finer or coarser sediments, respectively, and are regulated by the seasonality of the region. The dynamics of the fluctuating water table also plays an important role, especially in the formation of *Planossolos*. These soils typically occur in this type of terrain in the Brazilian semiarid region (Araújo Filho et al., 2020; Jacomine et al., 1975).

In this region, close to drainage channels, soils vary from deep (depth > 100 cm) soils with sandy texture (sand content > 850 g kg⁻¹) that are very porous and very permeable, which is the case of *Neossolos Rególicos*, to shallow (50 to 100-cm deep) or very shallow (depth < 50 cm) soils with medium or clayey texture that are imperfectly to poorly drained, with low infiltration rates. The latter may include *Planossolos* that present a compact argillic B horizon with lower permeability underneath a sandy, very porous E horizon with high permeability, as well as *Neossolos Litólicos* (Leptosols; Lythic Orthents or Psammments), which are very shallow soils with the regolith or underlying rock occurring before 50 cm. *Neossolos Flúvicos* present variable texture vertically along the profile, and thus, variable porosity and infiltration rates depending on the texture of the C (sediment) horizons.

The depth to the regolith varied between 81 (P9) and 160 cm (P5). The smallest depths to the regolith are located near the top of the slope at the northwest part of the area, while the largest are close to the dam at the southeast, as expected (Fig. 4, Table 1). Laterally, the deepest soils occur on the intermittent stream thalweg, as sediments coming from the side slopes accumulate in this zone. The processed and migrated radargrams plotted in 3D show the increase in the depth to the regolith along the top-to-dam direction (Fig. 4, red lines). This is expected, since sediments carried by seasonal rainwater and erosion processes move downslope and accumulate in the lower portion of the terrain, where the drainage channel narrows down, close to the proposed location for building the dam.

The plots of the individual radargrams show in more detail the shapes of the terrain surface and the top of the regolith, outlined with dashed black lines (Figs. 5 and 6). The Kirchhoff migration adjusted the radargrams to the shape of the terrain, as well as the reflections from the subsurface features to their original shapes. Thus, the radargrams transverse to the slope show the cross-sectional shape of the intermittent stream bed (Fig. 5), while the radargrams parallel to the slope show the longitudinal shape of the terrain and regolith (Fig. 6).

The position of the top of the regolith delineated in the radargrams matches almost precisely the position observed in the corresponding soil profiles, as shown by the black dashes in the radargrams, with a few exceptions (Figs. 5 and 6). The top of the regolith limits the soil profile (solum), and thus, the water reservoir at the bottom. Along the top-to-dam (downslope) direction, the depth to the regolith increases from about 94 cm (P8) to 130 cm (P1) close to the intermittent stream thalweg. Further from the thalweg, close to transect 13, the depth to the regolith starts at 81 cm at the upper slope (P9), reaches 100 cm at the midslope (P6), and 130 cm close to the dam (P3). Transverse to the slope, the depth to the regolith increases from the upper portion of the terrain (transect 13) towards the thalweg (transects 10 and 11), which is expected since more alluvial sediments accumulate closer to the thalweg. At the same time, the rainwater that seasonally flows down the stream digs the regolith deeper at the thalweg, resulting in a thicker soil profile.

The proposed location for building the dam and proposed dam length of about 65 m corresponds to the radargram taken at transect 1 (Figs. 2B and 5A). However, the radargram of transects 1 (dam) and 2 show that the intermittent stream thalweg occurs close to soil profile P1, and not

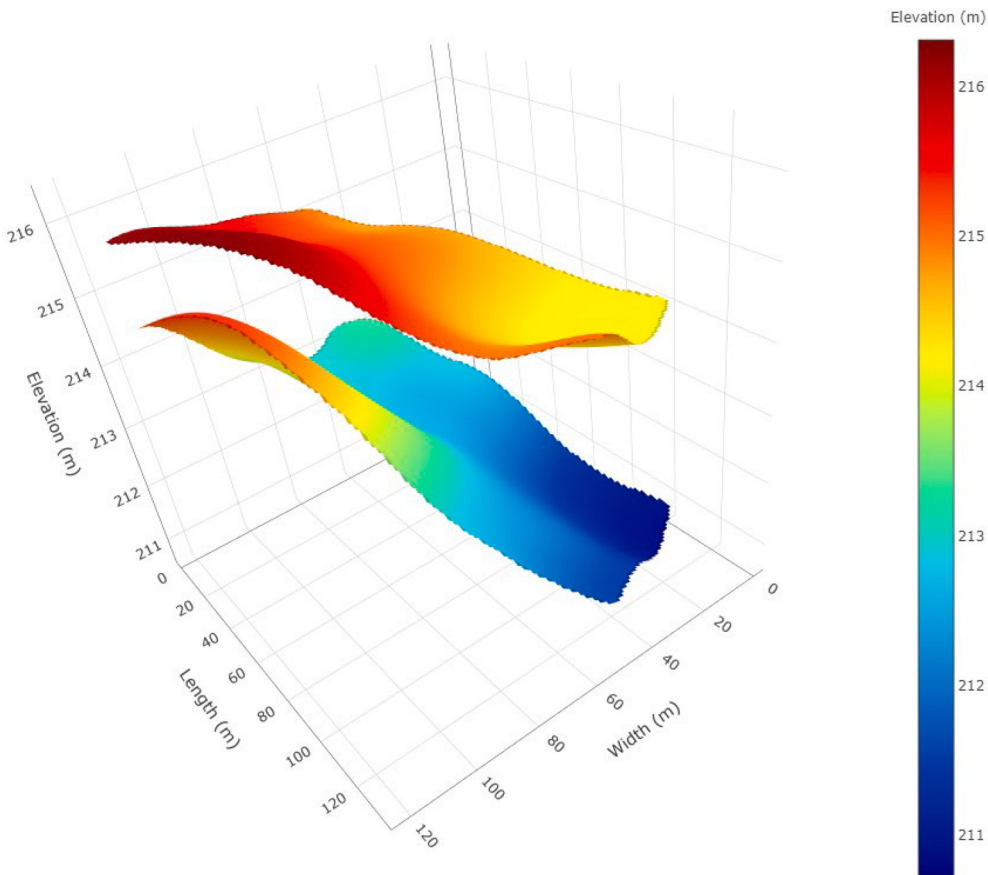


Fig. 7. 3D plot of the terrain surface and top of the regolith. The shape of the water reservoir is represented by the space between them. An interactive 3D plot can be accessed at https://rpubs.com/gmvasques/interactive_3D_plot_underground_dam_water_reservoir.

P2 as previously anticipated during the GPR survey (Fig. 5A and B). The GPR survey lines covered the area that was available to be flooded and used for cropping, which was initially proposed as the underground dam water accumulation area (Fig. 2B). At the southern border, close to transect 9, there is a rank of bushes that separate the study area from an adjacent area to the south. Initially, these bushes were to be preserved, but they could be cut down to expand the area. Therefore, it is recommended that the dam be extended about 45 m to the south, centering it about 22 m southwards, close to P1, provided that the southern portion of the study area can be used. This decision belongs to the landowner. Should this be done, and assuming that the cross-sectional shape of the slope is symmetrical, the terrain elevation and the depth to the regolith at the southern border of the accumulation area would be about the same as those at the northern border, close to transect 13, respectively.

3.2. Water accumulation area and water reservoir volume

The GPR allowed to identify, delineate and map the surface terrain, and the subsurface regolith, which were the features of interest. For that, the nine soil pits were used for ground truthing. For this study, the surface terrain limits the underground dam water reservoir at the top whereas the regolith limits the reservoir at the bottom. The GPR survey lines limit the reservoir on the sides and at the back. Thus, the GPR allowed to non-invasively characterize the shape of the underground dam water reservoir in 3D, and thus, estimate its volume. Many more soil pits would be required to do the same job. As such, the GPR minimized the need of soil sounding at the same time that it offered more precision and a 3D visualization of the reservoir.

The interpolated terrain surface elevation ranged between 213.5 and 215 m, and the elevation of the top of the regolith from 210 to 213.5 m,

from the dam to the upper slope, respectively (Fig. 7). The difference between the terrain surface elevation and the top of the regolith elevation constitutes the depth to the regolith, or the soil thickness, which constitutes the water reservoir thickness. Thus, the 3D shape of the water reservoir is represented by the space between the terrain surface and the top of the regolith. The water reservoir is thickest at the lowest portion of the slope close to the dam slopewise, and at the center close to the thalweg across (Fig. 7).

The study area of 8500 m² covered by the GPR survey lines was initially proposed as the water accumulation area of the underground dam. The water reservoir in this accumulation area lies between the terrain surface and the top of the regolith (Fig. 7) and its estimated volume is 10,561 m³. The water is stored in the soil pores, which occupy approximately 38% of the soil volume. Therefore, the total volume of the underground water reservoir is approximately 4013 m³. However, it was clear from the radargrams closer to the future dam location (Fig. 5A and B) that the proposed length of 65 m is too short and the proposed position is not centered at the stream thalweg. Thus, the length and position of the future dam should be revised by extending the dam and centering it correctly at the thalweg, allowing it to block more water, increase the accumulation area and avoid lateral leakage.

Therefore, extending the underground dam 45 m southwards to a total of 110 m in length, and centering it at the stream thalweg, as proposed, would increase the accumulation area to about 14,385 m², increase the total soil volume in the accumulation area about 50%, reaching 15,842 m³, and increase the water reservoir volume by 50% to about 6020 m³, which is equivalent to six thousand 1000-L or 12 thousand 500-L water tanks that are commonly used in small-family households in northeastern Brazil. More importantly, this would assert that the water is retained from flowing outwards laterally at the

southern border. Additionally, the top of the dam could be built above the terrain surface to store water aboveground for irrigation, animal watering, and other uses, and capture surface and runoff water during heavy rains.

4. Conclusions

The GPR as a non-invasive survey technology reduces the need for a large number of soil trenches and boreholes to assess the depth to soil restrictive layers, in this case, the regolith that limits the underground dam water accumulation area at the bottom. The radargrams allow identifying and mapping the main underground features, including the regolith, along the survey transects and, after interpolation, across the study area. The geographic coordinates and terrain surface elevation collected by the GPS receiver of the GPR are used for migrating the radargrams and interpolating the terrain surface and top of the regolith in 3D, allowing to visualize the shape of the underground dam water reservoir, and estimate its total volume.

The initial proposed location for building the dam is not centered at the intermittent stream thalweg position, as observed in the radargrams transverse to the slope. In addition, the initially proposed length of 65 m is not enough to block the water flow at the southern (lateral) portion of the slope at the same height of the northern border, which, in practice, makes the water reservoir much smaller than the estimated 4013 m³ as water is lost laterally. Therefore, extending the dam 45 m to the south, reaching a total length of 110 m, and centering it at the thalweg position, is recommended. This would increase the water reservoir volume by 50% to about 6020 m³. This increase is substantial and was only perceived from the GPR survey that showed the cross-sectional shape of the intermittent stream bed.

The analytical methods, functions, and tools provided by the free and open-source RGPR package in R covered the whole framework of GPR data handling and processing, including filtering, noise reducing, contrast enhancing, geolocating, migrating, feature identification and delineation, spatial interpolation, and 3D plotting. R is a science-oriented high-level programming language that is easy to learn, use and modify. The RGPR package is easy to install and use. Thus, using R and the RGPR package is recommended for its completeness and to reduce the cost of data analysis by replacing high-cost proprietary software. An online RGPR tutorial (<https://emanuelhuber.github.io/RGPR>) and a GitHub repository (<https://github.com/emanuelhuber/RGPR>) are available to aid users and developers.

Author statement

All persons who meet authorship criteria are listed as authors, and all authors certify that they have participated sufficiently in the work to take public responsibility for the content, including participation in the concept, design, analysis, writing, or revision of the manuscript.

Declaration of Competing Interest

The authors declare that they have no known competing financial interests or personal relationships that could have appeared to influence the work reported in this paper.

Data availability

The authors do not have permission to share data.

Acknowledgements

Funding was provided by the Brazilian Agricultural Research Corporation (Embrapa) project “Zoneamento edafoclimático participativo de áreas potenciais para construção de barragens subterrâneas em unidade agrícola de base familiar nas mesorregiões do Agreste e Sertão de Alagoas”

(Participatory edaphoclimatic zoning of potential areas for building underground dams in smallholder farms in the *Agreste* and *Sertão* regions of Alagoas state), grant number 26.16.04.002.00.00. The Federal Institute of Alagoas of Santana do Ipanema and Dr. Gilberto Gouveia Neto are acknowledged for their support.

References

- Afshar, F.A., Ayoubi, S., Castrignanò, A., Quarto, R., Ardekani, M.R.M., 2017. Using ground-penetrating radar to explore the cemented soil horizon in an arid region in Iran. *Near Surf. Geophys.* 15, 103–110. <https://doi.org/10.3997/1873-0604.2016049>.
- Apaydin, A., 2009. Malibogazi groundwater dam: an alternative model for semi-arid regions of Turkey to store and save groundwater. *Environ. Earth Sci.* 59, 339–345. <https://doi.org/10.1007/s12665-009-0030-8>.
- Aratujo Filho, J.C., Santos, J.C.P., Parahyba, R.B.V., Oliveira Neto, M.B., Barros, A.H.C., Marques, F.A., Amaral, A.J., 2020. Zoneamento Agroecológico do Estado de Alagoas: Levantamento de Reconhecimento de Baixa e Média Intensidade dos Solos do Estado de Alagoas. Embrapa Solos, Rio de Janeiro, Brazil. Documentos 216.
- Barros, A.H.C., Araújo Filho, J.C., Silva, A.B., Santiago, G.A.C.F., 2012. Climatologia do Estado de Alagoas. Embrapa Solos, 211. Boletim de Pesquisa e Desenvolvimento, Recife, Brazil.
- Bristow, C.S., Jol, H.M., 2003. Ground Penetrating Radar in Sediments. *Geological Society of London, London, United Kingdom. Geol. Soc. Spec. Publ.* 211.
- Cabral Júnior, J.B., Bezerra, B.G., 2018. Análises da evapotranspiração de referência e do índice de aridez para o Nordeste do Brasil. *Rev. Geoci. Nordeste* 4, 71–89. <https://doi.org/10.21680/2447-3359.2018v4n1ID14746>.
- Castro, D.L., Júnior, J.A.R., Teixeira, W.L.E., Silva, V.A., Filho, F.P.L., 2014. Ground-Penetrating radar imaging techniques applied in 3D environment: example in inactive dunes. *Rev. Bras. Geofis.* 32, 1–17. <https://doi.org/10.22564/rbgf.v32i2.482>.
- Daniels, J.J., 1989. Fundamentals of Ground Penetrating Radar. In: Symposium on the Application of Geophysics to Engineering and Environmental Problems, 89, pp. 62–142. <https://doi.org/10.4133/1.2921864>. Golden, USA.
- Davis, J.L., Annan, A.P., 1989. Ground-penetrating radar for high-resolution mapping of soil and rock stratigraphy. *Geophys. Prospect.* 37, 531–551. <https://doi.org/10.1111/j.1365-2478.1989.tb02221.x>.
- Doolittle, J.A., 1982. Characterizing soil map units with the ground-penetrating radar. *Soil Survey Horizons* 23, 3–10. <https://doi.org/10.2136/sh1982.4.0003>.
- Doolittle, J.A., Jenkinson, B., Hopkins, D., Ulmer, M., Tuttle, W., 2006. Hydropedological investigations with ground-penetrating radar (GPR): estimating water-table depths and local ground-water flow pattern in areas of coarse-textured soils. *Geoderma* 131, 317–329. <https://doi.org/10.1016/j.geoderma.2005.03.027>.
- Douglas, D.G., Burns, A.A., Rino, C.L., Maresca, J.W., Yezzi, J.J., 1992. A Study to Determine the Feasibility of Using a Ground-Penetrating Radar for More Effective Remediation of Subsurface Contamination. United States Environmental Protection Agency, Washington, DC, USA. EPA/600/SR-92/089.
- Dujardin, J.-R., Bano, M., 2013. Topographic migration of GPR data: examples from Chad and Mongolia. *Comptes Rendus Geosci.* 345, 73–80. <https://doi.org/10.1016/j.crte.2013.01.003>.
- El-Hames, A.S., 2012. Determination of the transient water table rise behind constructed underground dams. *Arab. J. Geosci.* 5, 1359–1366. <https://doi.org/10.1007/s12517-011-0299-2>.
- Ertsen, M., Hut, R., 2009. Two waterfalls do not hear each other. Sand-storage dams, science and sustainable development in Kenya. *Phys. Chem. Earth, Parts A/B/C* 34, 14–22. <https://doi.org/10.1016/j.pce.2008.03.009>.
- Fan, B., Liu, X., Zhu, Q., Qin, G., Li, J., Lin, H., Guo, L., 2020. Exploring the interplay between infiltration dynamics and critical Zone structures with multiscale geophysical imaging: a review. *Geoderma* 374, 114431. <https://doi.org/10.1016/j.geoderma.2020.114431>.
- Finley, A., Banerjee, S., Hjelle, Ø., 2017. *MBA: Multilevel B-Spline Approximation. R Package Version 0.0-9*.
- Forzieri, G., Gardenti, M., Caparrini, F., Castelli, F., 2008. A methodology for the pre-selection of suitable sites for surface and underground small dams in arid areas: a case study in the region of Kidal, Mali. *Phys. Chem. Earth, Parts A/B/C* 33, 74–85. <https://doi.org/10.1016/j.pce.2007.04.014>.
- Freeland, R.S., Yoder, R.E., Ammons, J.T., 1998. Mapping shallow underground features that influence site-specific agricultural production. *J. Appl. Geophys.* 40, 19–27. [https://doi.org/10.1016/S0926-9851\(98\)00014-7](https://doi.org/10.1016/S0926-9851(98)00014-7).
- Gerber, R., Felix-Henningsen, P., Behrens, T., Scholten, T., 2010. Applicability of ground-penetrating radar as a tool for nondestructive soil-depth mapping on pleistocene periglacial slope deposits. *J. Plant Nutr. Soil Sci.* 173, 173–184. <https://doi.org/10.1002/jpln.200800163>.
- Gomes, J.L.S., Vieira, F.P., 2020. Electrical resistivity survey combining multiple electrode arrays applied to the studies of underground dams. *Int. J. Geosci. Eng. Technol.* 2, 160–165.
- Huber, E., Hans, G., 2019. RGPR: Ground-penetrating radar (GPR) Data Visualisation, Processing and Delineation. R package version 0.0.7.
- IBGE (Instituto Brasileiro de Geografia e Estatística), 2019. Brasil - Unidades da Federação 2019. Shapefile, 1, p. 250,000.
- Ishida, S., Kotoku, M., Abe, E., Fazal, M.A., Tsuchihara, T., Masayuki, I., 2003. Construction of subsurface dams and their impact on the environment. *Mater. Geoenviron.* 50, 149–152.

- Ishida, S., Tsuchihara, T., Yoshimoto, S., Imaizumi, M., 2011. Sustainable use of groundwater with underground dams. *Japan Agric. Res. Quart.* 45, 51–61. <https://doi.org/10.6090/jarq.45.51>.
- IUSS Working Group WRB, 2015. *World Reference Base for Soil Resources 2014, Update 2015: International Soil Classification System for Naming Soils and Creating Legends for Soil Maps*. FAO, Rome, Italy (World Soil Resources Reports 106).
- Jacomine, P.K.T., Cavalcanti, A.C., Silveira, C.O., Pessôa, S.C.P., 1975. Levantamento exploratório-reconhecimento de solos do Estado de Alagoas. Embrapa-CPP, Recife, Brazil. Boletim Técnico, 35.
- Knight, R., 2001. Ground penetrating radar for environmental applications. *Annu. Rev. Earth Planet. Sci.* 29, 229–255. <https://doi.org/10.1146/annurev.earth.29.1.229>.
- Lima, A.D.O., Dias, N.D.S., Ferreira Neto, M., Santos, J.E.J., Rego, P.R., Lima-Filho, F.P., 2013. Barragens subterrâneas no Semiárido brasileiro: Análise histórica e metodologias de construção. *Irriga* 18, 200–211. <https://doi.org/10.15809/irriga.2013v18n2p200>.
- Lima, A.O., Lima-Filho, F.P., Dias, N.S., Júnior, J.A.R., Sousa, A.M., 2018. GPR 3D profile of the adequateness of underground dams in a sub-watershed of the Brazilian semiarid. *Rev. Caatinga* 31, 523–531. <https://doi.org/10.1590/1983-21252018v31n230r>.
- Liu, X., Dong, X., Leskovar, D.I., 2016. Ground penetrating radar for underground sensing in agriculture: a review. *Int. Agrophys.* 30, 533–543. <https://doi.org/10.1515/intag-2016-0010>.
- Loperte, A., Bavusi, M., Cervizzzo, G., Lapenna, V., Soldovieri, F., 2011. Ground penetrating radar in dam monitoring: the test case of Acerenza (Southern Italy). *Int. J. Geophys.* 2011, 654194 <https://doi.org/10.1155/2011/654194>.
- Lopes, H.L., Cabral, J.J.S.P., Araújo Filho, J.C., Montenegro, S.M.G.L., 2013. Mapeamento de áreas aluvionares no semiárido brasileiro por meio de dados colaterais e imagens orbitais. *Rev. Bras. Eng. Agríc. Amb.* 17, 763–769. <https://doi.org/10.1590/s1415-43662013000700011>.
- Nascimento, C.W.R., Rodrigues, H.M., Ceddia, M.B., Vasques, G.M., Oliveira, S.M., Figueira, H.F.V., 2019a. Identificação de limites entre duas classes de solo utilizando radar de penetração no solo com profundidades ajustadas por barras de ferro e validação com trado holandês. In: Simpósio Brasileiro de Geografia Física Aplicada, 18, Fortaleza, Brazil, 11.
- Nascimento, C.W.R., Rodrigues, H.M., Ceddia, M.B., Vasques, G.M., Oliveira, S.M., Santos, W.M., Freire, M.D.O., 2019b. Identificação em profundidade de barras de ferro utilizando radar de penetração do solo (GPR) com antena de 450 MHz em três classes de solo. In: Simpósio Brasileiro de Geografia Física Aplicada, 18, p. 12. Fortaleza, Brazil.
- Nováková, E., Karous, M., Zajíček, A., Karousová, M., 2013. Evaluation of ground penetrating radar and vertical electrical sounding methods to determine soil horizons and bedrock at the locality Dehtáře. *Soil Water Res.* 8, 105–112. <https://doi.org/10.17221/6/2012-swrr>.
- Onder, H., Yilmaz, M., 2005. Underground dams. A tool of sustainable development and management of groundwater resources. *Eur. Water* 11–12, 35–45.
- Pueyo Anchuela, O., Frongia, P., Di Gregorio, F., Casas Sainz, A.M., Pocoví Juan, A., 2018. Internal characterization of embankment dams using ground penetrating radar (GPR) and thermographic analysis: a case study of the Medau Zirimilis Dam (Sardinia, Italy). *Eng. Geol.* 237, 129–139. <https://doi.org/10.1016/j.enggeo.2018.02.015>.
- Quilis, R.O., Hoogmoed, M., Ertsen, M., Foppen, J.W., Hut, R., Vries, A., 2009. Measuring and modeling hydrological processes of sand-storage dams on different spatial scales. *Phys. Chem. Earth, Parts A/B/C* 34, 289–298. <https://doi.org/10.1016/j.pce.2008.06.057>.
- R Core Team, 2020. R: A Language and Environment for Statistical Computing. R Foundation for Statistical Computing, Vienna, Austria.
- Rodrigues, H.M., Nascimento, C.W.R., Ceddia, M.B., Vasques, G.M., Nunes, J.F., Santos, F.B., 2019. Uso de barras de ferro para diferenciação entre horizontes de três classes de solo utilizando radar de penetração do solo (GPR) com antena monostática de 750 MHz. In: Simpósio Brasileiro de Geografia Física Aplicada, 18, Fortaleza, Brazil, 12.
- Santos, R.D., Santos, H.G., Ker, J.C., Anjos, L.H.C., Shimizu, S.H., 2015. Manual de Descrição e Coleta de Solo no Campo, 7th ed. Sociedade Brasileira de Ciência do Solo, Viçosa, Brazil.
- Santos, H.G., Jacomine, P.K.T., Anjos, L.H.C., Oliveira, V.A., Lumbreiras, J.F., Coelho, M. R., Almeida, J.A., Araújo Filho, J.C., Oliveira, J.B., Cunha, T.J.F., 2018. Sistema Brasileiro de Classificação de Solos, 5th ed. Embrapa, Brasília, Brazil.
- Sass, O., 2007. Bedrock detection and talus thickness assessment in the European Alps using geophysical methods. *J. Appl. Geophys.* 62, 254–269. <https://doi.org/10.1016/j.jappgeo.2006.12.003>.
- Silva, A.S., Porto, E.R., 1982. Utilização e Conservação dos Recursos Hídricos nas Zonas Rurais do Trópico Semi-Árido do Brasil: Tecnologias de Baixo Custo. Embrapa, Petrolina, Brazil. Documentos 14.
- Silva, M.S.L., Lopes, P.R.C., Anjos, J.B., Silva, A.S., Brito, L.T.L., Porto, E.R., 1998. Exploração agrícola em barragem subterrânea. *Pesqui. Agropecu. Bras.* 33, 975–980.
- Silva, M.S.L., Ferreira, G.B., Lucena, A.M.A., Oliveira Neto, M.B., Parahyba, R.B.V., Santos, J.C.P., Cunha, T.J.F., 2009. Limitações e potencialidades de classes de solos para locações de barragens subterrâneas no Semiárido do Nordeste. In: Congresso Brasileiro de Ciência do Solo, 32, Fortaleza, Brazil, 5.
- Silva, M.S.L., Parahyba, R.B.V., Oliveira Neto, M.B., Leite, A.P., Santos, J.C.P., Cunha, T. J.F., Moreira, M.M., Ferreira, G.B., Anjos, J.B., Melo, R.F., 2010. Potencialidades de classes de solos e critérios para locação de barragens subterrâneas no Semiárido do Nordeste brasileiro. Embrapa Solos, Recife, Brazil. Circular Técnica 45.
- Soil Survey Staff, 2014. Keys to Soil Taxonomy, 12th ed. USDA, Natural Resources Conservation Service, Washington, DC, USA.
- Ximenes, L.F., Silva, M.S.L., Brito, L.T.L., 2019. Tecnologias de convivência com o semiárido brasileiro. Banco do Nordeste do Brasil, Fortaleza, Brazil.